CARBON letters

Original Articles
Carbon Letters Vol. 24, 90-96 (2017)

Optical sensitivity of DNA-dispersed single-walled carbon nanotubes within cement composites under mechanical load

Jin Hee Kim[1], Inkyu Rhee[2,♠], Yong Chae Jung[3], Sumin Ha[4] and Yoong Ahm Kim[4,♠]

[1]Faculty of Engineering, Chonnam National University, Gwangju 61186, Korea
[2]Department of Civil Engineering, Chonnam National University, Gwangju 61186, Korea
[3]Multifunctional Structural Composite Research Center, Institute of Advanced Composite Materials, Korea Institute of Science and Technology (KIST), Jeonbuk 55324, Korea
[4]School of Polymer Science and Engineering, Department of Polymer Engineering, Graduate School & Alan G. MacDiarmid Energy Research Institute, Chonnam National University, Gwangju 61186, Korea

Article Info

Received 16 May 2017
Accepted 9 June 2017

♠Corresponding Author
E-mail: rheei@jnu.ac.kr
yak@jnu.ac.kr
Tel: +82-62-530-1653
+82-62-530-1871

Open Access

DOI: http://dx.doi.org/10.5714/CL.2017.24.090

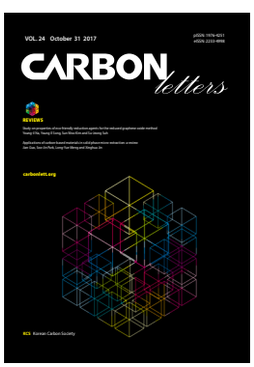

http://carbonlett.org

pISSN: 1976-4251
eISSN: 2233-4998

Abstract

We demonstrated the sensitivity of optically active single-walled carbon nanotubes (SWCNTs) with a diameter below 1 nm that were homogeneously dispersed in cement composites under a mechanical load. Deoxyribonucleic acid (DNA) was selected as the dispersing agent to achieve a homogeneous dispersion of SWCNTs in an aqueous solution, and the dispersion state of the SWCNTs were characterized using various optical tools. It was found that the addition of a large amount of DNA prohibited the structural evolution of calcium hydroxide and calcium silicate hydrate. Based on the in-situ Raman and X-ray diffraction studies, it was evident that hydrophilic functional groups within the DNA strongly retarded the hydration reaction. The optimum amount of DNA with respect to the cement was found to be 0.05 wt%. The strong Raman signals coming from the SWCNTs entrapped in the cement composites enabled us to understand their dispersion state within the cement as well as their interfacial interaction. The G and G' bands of the SWCNTs sensitively varied under mechanical compression. Our results indicate that an extremely small amount of SWCNTs can be used as an optical strain sensor if they are homogeneously dispersed within cement composites.

Key words: cement composite, single walled carbon nanotube, DNA, compressive strength, Raman

1. Introduction

Cement composites are one of the most widely used construction materials in buildings due to their low cost and high compressive strength [1]. However, intrinsic problems such as mechanical brittleness and electrical insulating properties are some of the challenging issues that need to be addressed. In this regard, extensive studies have been conducted on the addition of nanosized materials (e.g., silica, titanium oxide, carbon nanotubes [CNTs] and graphenes) to cement composites [2-16]. This is because nanomaterials can restrict the growth of nanosized cracks in cement composites to microsized ones.

Among the various nanomaterials, one-dimensional CNTs have been intensively examined as a reinforcing filler of cement composites due to their high aspect ratio (up to 10,000) as well as their excellent mechanical, thermal and electrical properties [6-18]. Morphologically, CNTs consist of single or multiple concentric graphene cylinders, and they are distinguished as single, double and multi-walled carbon nanotubes (SWCNTs, DWCNTs and MWCNTs) depending upon the number of walls present [19,20]. The purpose of using CNTs as a functional filler is to improve the mechanical and electrical properties as well as provide a piezoresistive property to cement composites [6-18]. However, no systematic study has

been done to date on the optical sensitivity of SWCNTs within cement composites under mechanical compression even though SWCNTs with a diameter less than 1 nm exhibit extremely strong but sensitive optical properties due to the quantum confinement effect. Small-sized CNTs can be easily aggregated to generate large-sized bundles due to strong van der Waals interactions between adjacent tubes. Thus, to exploit the intrinsic properties of SWCNTs, various organic molecules have been used to disperse or segregate them in an aqueous solution [21]. On the other hand, to exploit their excellent physical and optical properties in biological fields, various types of biomaterials have been examined as dispersing agents for CNTs [22-27].

In the present work, to prepare an aqueous nanotube suspension, deoxyribonucleic acid (DNA) was selected as a dispersing agent because of its high dispersing ability with regard to bundled nanotube structures by wrapping the DNA onto their sidewall. Thus, DNA molecules can be expected to change the hydration reaction of cements resulting in a variation of the mechanical properties of cement composites. The effect of DNA molecules on the hydration reaction was evaluated using combined in situ Raman and X-ray diffraction (XRD) studies. Finally, we demonstrated the sensing ability of the optically active SWCNTs that were homogeneously dispersed in cement composites under mechanical compression.

2. Experimental

Highly purified HiPco-based SWCNTs with a diameter below 1 nm were used as a functional filler in cement composites [28]. To prepare a nanotube suspension, solid-state nanotubes were dispersed in an aqueous solution with the help of DNA (herring sperm, Sigma Aldrich, USA) under strong sonication (Kubota UP50H, 130 W cm^{-2}, amplitude 60%) for 1 h at room temperature and subsequent ultracentrifugation (Optima Max-XP, Beckman Coulter, USA; 120,000g). The dispersion state of the SWCNTs in solution was optically evaluated with Raman spectroscopy (785 nm), UV-visible absorption (SolidSpec-3700, Shimazu, Japan) and photoluminescence (NIR-PL system, Shimazu).

We used ordinary Portland cement as the main component in the fabrication of the cement composites and fixed the water-to-cement ratio at 0.35 for a direct comparison. To understand the effect of DNA on the microstructure and physical properties of the cement composites, the cement composites consisting of cement and water containing DNA (0.025, 0.05, 0.075, 0.1 and 0.5 wt%) were molded into a cylinder (diameter, 2.5 cm; height, 5 cm).

Cement pastes consisting of cement and water containing DNA (0.025, 0.05, 0.075, 0.1 and 0.5 wt%) were mixed homogeneously for 5 min and then transferred to a glass petri dish. Then, Raman measurements were carried out under atmospheric condition (25°C and 35% relative humidity) using a Raman spectrometer (532 nm laser line, Nanobase Inc., Korea). In all cases, the laser power was below 5 mW to avoid the laser heating effect on the samples. The hydration age was counted from the time when the cement and the water containing DNA were mixed.

The microstructure including the shape of the hydration crystals were observed using field-emission scanning electron microscopy (FE-SEM). The cement composites were ground into a fine powder and then sieved to obtain the XRD patterns (D-Max-2400 diffractometer, CuK_{α} radiation [λ= 0.15418 nm]). The compressive strength of the cement composites was measured using ASTM C39 and KS F 2405.

Cement pastes consisting of cement and a DNA-dispersed SWCNT suspension were molded into a cube (1×1×1 cm). Note that the water-to-cement ratio was fixed at 0.35; the added amount of DNA was 0.05 wt%, and the added amount of SWCNTs was 0.005 wt%. The mold was removed after 24 h and then cured for 14 d to evaluate the possibility of using dispersed SWCNTs within cement composites as an optical sensor using Raman spectroscopy under a mechanical load.

3. Results and Discussion

Highly purified SWCNTs with an extremely high aspect ratio above 10,000 can be easily aggregated due to the strong van der Waals interactions between adjacent tubes. The SWCNTs have a large bundle size in the range 20–50 nm, in which each tube has a diameter of 0.4–1.2 nm [28]. Therefore, to exploit the intrinsic properties of SWCNTs, it is critical to disperse (or disentangle) them into individual tubes in an aqueous solution. In our previous works, DNA was selected as a dispersing agent due to its high dispersing ability with regard to CNTs by helical wrapping onto the sidewall [25-27]. The DNA solution containing the nanotube sample was sonicated using a horn-type sonicator for 1 h. A visual change from a transparent to an opaque suspension could be observed before and after sonication, respectively (Fig. 1a). Of note, no sedimentation occurred for 1 mo. To evaluate the dispersion state of SWCNTs in an aqueous solution, we obtained the Raman spectra using a 785 nm laser line (Fig. 1b). A highly intensified G-band (E_{2g2} mode) at 1590 cm^{-1}, ra-

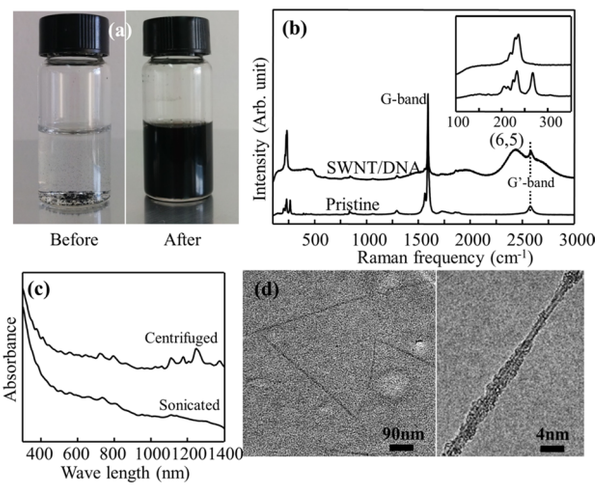

Fig. 1. (a) Optical images of the single-walled carbon nanotubes (SWCNT) suspension containing DNA before and after sonication, (b) Raman and fluorescent spectra obtained using a 785 nm laser line for the pristine SWCNTs and DNA-dispersed SWCNT suspension, (c) ultraviolet absorption spectrum of the DNA-dispersed SWCNT suspension before and after centrifugation, (d) transmission electron microscope images of individual SWCNTs with helical wrapping of DNA at different magnifications.

dial breathing modes (RBMs) below 350 cm^{-1} and second-order symmetry enabling a G'-band at 2600 cm^{-1} were observed from the pristine SWCNT sample. From the sonicated suspension, the appearance of a strong luminescence peak around 2500 cm^{-1} indicated the presence of isolated (or individual) SWCNT with a chirality of (6,5) from the helical wrapping of DNA. It has been already reported that the absence of luminescent signals from a bundled structure is due to the presence of metallic SWCNTs [29]. In low-frequency Raman spectra (inset in Fig. 1b), we observed a largely depressed RBM at 267 cm^{-1} and an increased intensity of RBM at 234 cm^{-1} indicating the individualization of the SWCNTs in the aqueous solution with the aid of DNA [30,31]. Moreover, compared to the sonicated suspension, the observation of well-resolved optical absorption peaks arising from their excitonic transitions between van Hove singularities also indicated the individualization of the SWCNTs in the centrifuged suspension (Fig. 1c). Visually, transmission electron microscopy (TEM) micrographs showed the isolated SWCNTs with a coating of DNA (Fig. 1d).

As noted in Fig. 1d, the helical wrapping of DNA enabled the SWCNTs to be isolated in an aqueous solution. Thus, it would be logical to consider the effect of DNA on the microtexture of hardened cement composites consisting of complex cement hydration reaction products (e.g., ettringite, monosulfonate, calcium hydroxide and calcium silicate hydrate [C-S-H] gel) [32]. Thus, we carried out a detailed SEM observation to see the difference in the evolution of cement hydration crystals on fractured pristine and cement composites which were cured for 6 and 30 d, respectively. For the pristine sample, we observed well developed plates (calcium hydroxide) and needles (ettringite) (Fig. 2a). When 0.1 wt% of DNA was added to the cement paste, there was a clear decrease in both the size and density of the plates and needles. In contrast, it was very hard to see the plates and needles for the cement composites containing 0.5 wt% of DNA. The SEM micrographs showed that the addition of DNA hampered the cement hydration reaction. It was also important to evaluate the presence of C-S-H in our cement composites because C-S-H has a high ability to bind cement particles as a continuous phase making cured cement strong and durable [33]. For the pristine cement, sea urchin-like particles 2-3 μm in size were found on the outer surface of the original particle boundaries as well as high density needles (Fig. 2b). The number of needles decreased as the amount of added DNA was increased. There was no distinctive change in the C-S-H formation before and after the addition of the DNA at the microscale level. Eventually, for the cement hydration reaction, an excessive addition of DNA largely perturbed the formation of hydrated crystals possibly due to the large number of hydrophilic functional groups on the DNA.

There is a close relationship between the morphology and density of the hydrated crystals and the mechanical property of the hardened cement composites [30]. Therefore, to support our assumption on the perturbation effect due to an excess amount of added DNA, the compressive strengths of pristine and cement composites containing various amounts of DNA were evaluated. Visually, there was no distinctive change in the appearance of the cylinder-type sample before and after the addition of DNA (Fig. 3a). Noticeably, we achieved the highest compressive strength upon the addition of 0.05 wt% of DNA. When a small amount of

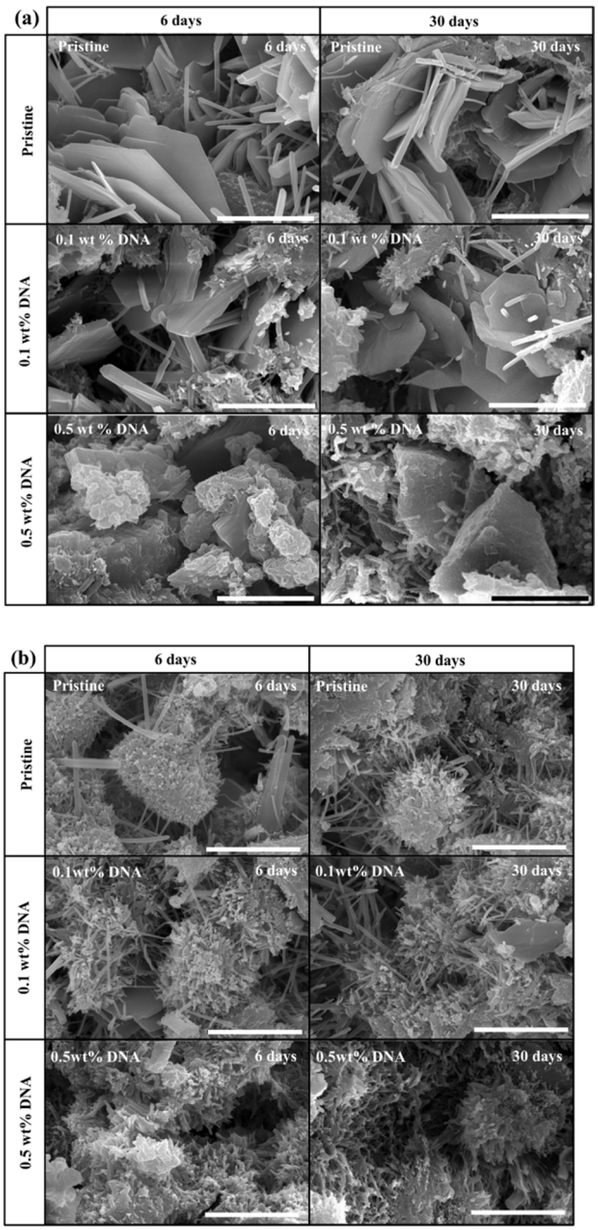

Fig. 2. Scanning electron microscopic images of (a) calcium hydroxide and (b) calcium silicate hydrate for the pristine- and DNA-added cement composites cured 6 and 30 d, respectively. Note that the scale bar is 3 μm.

DNA (below 0.075 wt%) was added, the compressive strength of the cement composites was higher than that of the pristine cement. We expected that the small amount of DNA would not hamper both the shape and the amount of the hydrated crystals in the hardened cement composites. However, when a higher amount of DNA (above 0.1 wt%) was added, the compressive strength of the cement composites decreased significantly due to the perturbation effect of the DNA. This result indicates that a large amount of DNA can largely impede the formation of hydrated crystals resulting in a deteriorated compressive strength of the cement composites.

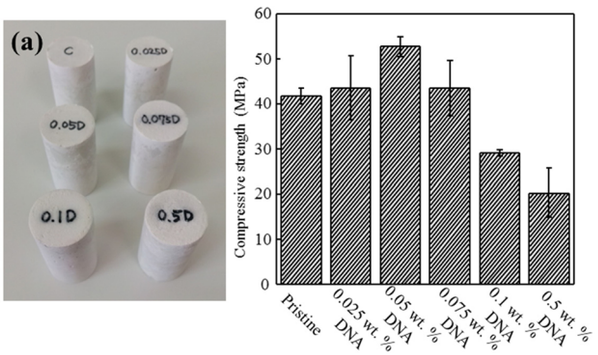

Fig. 3. (a) Photos showing the cylinder-type cement composites containing various amounts of DNA and (b) their corresponding compressive strengths. Note that the cement composite containing 0.05 wt% of DNA showed the highest compressive strength.

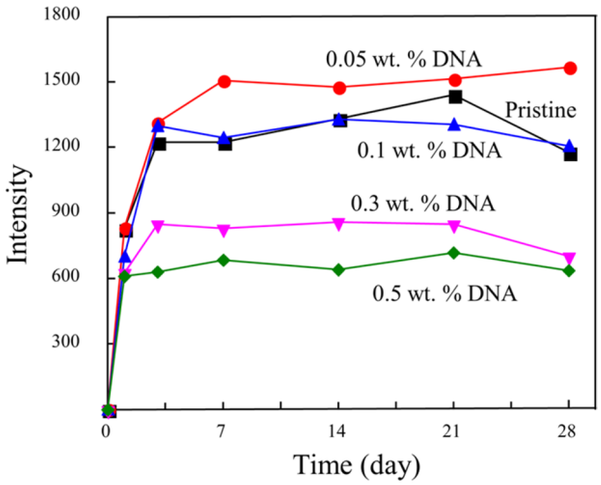

Fig. 4. Variation of the diffracted intensity of calcium hydroxide for cement composites containing various amounts of DNA as a function of the curing time.

To understand the variation in the compressive strength of the cement composites as a function of the added amount of DNA, XRD was done on the pristine and cement composites containing various amounts of DNA. First, we monitored the time-dependent change in the XRD patterns of the pristine cement and DNA added cement composites at 1, 3, 5, 14, 21 and 28 d (Fig. S1). The hardened cement consisted of various types of crystallites, such as unhydrated silicates, calcium hydroxide and ettringite. Thus, the diffracted peaks coming from the various crystallites overlapped with each other making it difficult to distinguish them clearly. Fortunately, the diffracted peak at 18° coming from calcium hydroxide did not overlap, and thus, we plotted the intensity of this diffracted peak as a function of the curing time (Fig. 4). For small samples, the intensities of the peaks at 18° first showed an abrupt increase on day 1, and then, they levelled off after 3 d. Interestingly, the diffracted intensity of this peak for the pristine and cement composites containing 0.01 and 0.05 wt% of DNA was two times higher than that of the cement composites containing 0.3 and 0.5 wt% of DNA. This result was consistent with the compressive strength of the cement composites containing various amounts of added DNA (Fig. 3b). From this result, we believe that the excessively added amount of DNA hindered the early hydration process so that less hydration products (e.g., C-S-H, calcium hydroxide, ettringite, etc.) were developed. However, this retardation phenomenon was recovered eventually (see the Raman spectra results after 5 mo of curing in Fig. S2). Compared with C-S-H, the strength-contributing potential of calcium hydroxide is limited due to its considerably lower surface area. Because a noticeable change in the XRD pattern was only observed in calcium hydroxide, the hydration degree was indirectly estimated by means of the intensity of the calcium hydroxide.

For early curing times from 1 to 8 h, we carried out in-situ Raman measurements on the pristine and cement composites containing 0.5 wt% of DNA (Fig. 5). The Raman spectra of the pristine cement sample (Fig. 5a) showed two sharp bands at 253 and 356 cm^{-1} and a broad band at 680 cm^{-1} coming from the calcium hydroxide [34]. With an increasing curing time, the intensity of these three bands for calcium hydroxide increased linearly. In contrast, no Raman bands coming from calcium hydroxide were observed for the cement composites containing 0.5 wt% of DNA (Fig. 5b). This result also supported the perturbation effect of the DNA on the formation of calcium hydroxide. Similarly, the growth of ettringite was evaluated by the band at 988 cm^{-1} for the pristine cement sample. However, there was no significant change in the ettringite Raman bands for cement composites containing 0.5 wt% of DNA. Furthermore, there is no broad symmetric stretching motion of the Si-O-Si mode near 660 cm^{-1} due to the low crystallinity of the C-S-H. [34] For the cement composites containing DNA (Fig. 5b), we did not observe any distinctive change in the Raman spectra during the curing time from 1 to 4 h. However, a subtle change in the Raman spectra could be observed during the curing time from 5 to 8 h. This result can be explained by the delayed start of the hydration reaction due to the addition of DNA which shows the perturbation effect of the DNA. To understand the effect of DNA on the hydration reaction, we compared the Raman spectra of the cement powder and the cured cement composites containing 0.5 wt% of DNA at 5 mo (Fig. S2). Interestingly, no large difference in the Raman spectra between the two samples were seen which supports the perturbation effect of excessively entrapped DNA on the hydration reaction of cement.

Finally, a SWCNT-filled cement composite was molded into a cube (1×1×1 cm) to verify the possibility of using the entrapped SWCNTs as an optical sensor under mechanical compression. Based on our detailed study on the effect of DNA, we optimized the added amount of DNA to 0.05 wt% with regard to the cement particles (see the compressive strength of the cement composites in Fig. 3). Therefore, we prepared the nanotube suspension by adding a very small amount of SWCNTs (ca. 0.005 wt%) to the DNA solution followed by ultra-sonication for 1 h. Next, the opaque SWCNT suspension (see the optical image on the right in Fig. 1a) was poured into the cement particles and then mixed thoroughly for 10 min. The cement paste was molded to a cubical shape. For all cases, the water-to-cement ratio was fixed to 0.35. As shown in the inset of Fig. 6a, there was no color change in the cement sample because the added

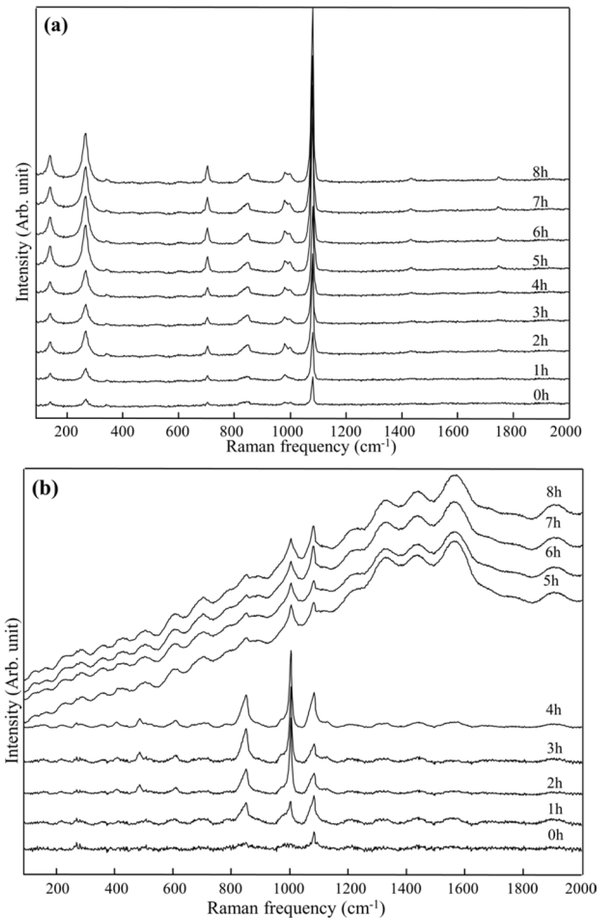

Fig. 5. In-situ Raman spectra of the (a) pristine and (b) cement composite containing 0.5 wt% of DNA at an early state of the hydration reaction from 1 to 8 h. Note that water-to-cement ratio was fixed at 0.35.

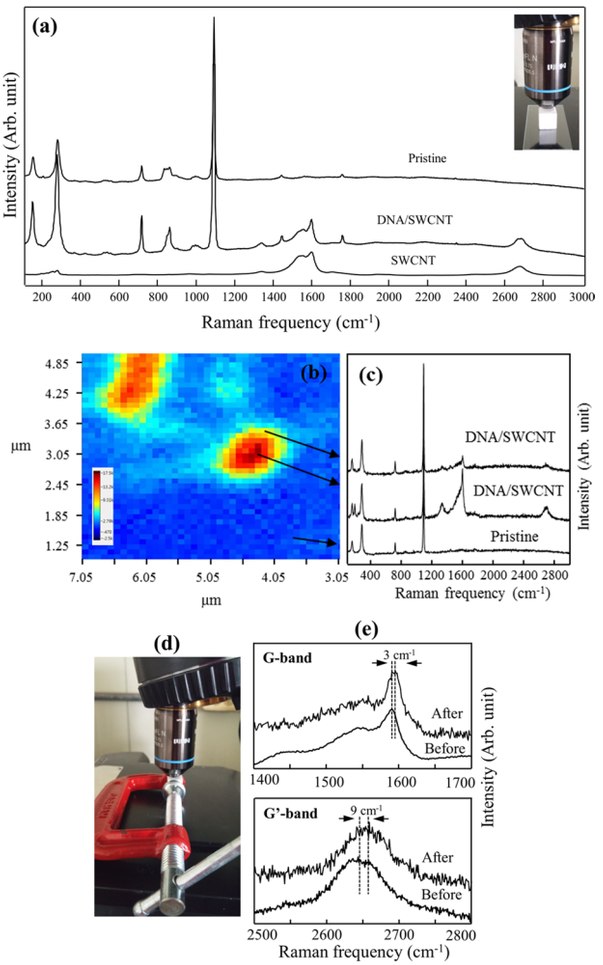

Fig. 6. (a) Raman spectra of the single-walled carbon nanotubes (SWCNTs), cement composites containing DNA and DNA-dispersed SWCNTs (Inset is a photo showing the cubic type cement composite under an optical microscope); (b) Raman spectra image of the DNA-dispersed SWCNT-filled cement composites and (c) their corresponding Raman spectra (note that Raman images are obtained from the integrated intensity over the G-band of the SWCNTs); and (d) photos showing the in-situ Raman setup under a mechanical load and (e) Raman spectra of the cement composites containing DNA-dispersed SWCNTs before and after mechanical compression. Note that the laser line is at 532 nm.

amount of SWCNTs was extremely small (ca. 0.005 wt%), and the diameter of the highly dispersed SWCNTs was below 1 nm (visually transparent to the naked eye). Fig. 6a shows the Raman spectra of the SWCNTs, the pristine cement and the DNA-dispersed SWCNT-filled cement composites. A strong peak (G-band) around 1590 cm^{-1} and a broad peak (G'-band) around 2650 cm^{-1} were ascribed to the highly dispersed SWCNTs within the cement matrix. Compared with the SWCNTs, the depressed Breit-Wigner-Fano line around 1550 cm^{-1} and the asymmetric shape of the G'-band were attributed to the presence of wrapped DNA, which induced a transition from metallic to p-type semiconducting SWCNTs [35,36]. To evaluate the dispersion state of the SWCNTs in the cement composite, large area Raman image (3×4 μm) (Fig. 6b) and their corresponding Raman spectra (Fig. 6c) were obtained. As seen in the spatially resolved Raman image (Fig. 6b), we clearly noticed the presence of SWCNTs in this region. The Raman spectrum in dark red showed two characteristic Raman bands from the SWCNTs (i.e., G-band and G'-band) as well as several Raman bands from hydrated crystals below 1200 cm^{-1}. The yellow region showed the decreased Raman intensities of the G- and G'-bands relative to the intensities of the Raman bands from the hydrated crystals. However, there is no Raman band from the SWCNTs in the blue region. When considering the laser spot size (1 μm) for obtaining Raman imaging, individual SWCNTs are spatially separated from each other. Due to the resonance effect of the SWCNTs, it is possible to see the spatial distribution of the SWCNTs within the cement composites from the Raman mapping.

Moreover, to evaluate the optical changes in the entrapped SWCNTs within the cement matrix under a mechanical load, the cubic-type sample was clinched on a handle-type vice (2 inch) followed by placing a 50× magnification objective from the Raman apparatus onto the sample (Fig. 6d). Mechanical compression was applied to the cubic-type cement composite by rotating the handle bar of the vice three quarters of a turn (0.75 mm)

DOI: http://dx.doi.org/10.5714/CL.2017.24.090

to manipulate the longitudinally strained cube specimen. The maximum compressive strength was measured to be ca. 3.77 kN when the cube specimen failed at a 0.92 mm downward displacement longitudinally (see Fig. S3). Then, we obtained the Raman spectra of the cement composites containing the DNA-dispersed SWCNTs before and after the mechanical compression. Interestingly, we observed upshifted Raman bands due to the mechanical compression from the cement matrix. A shift of 2–4 cm^{-1} for the G band and 5–10 cm^{-1} for the G' band were observed in our compression-experienced samples (Fig. 6e). The transferred pressure from the cement matrix induced upshifts of the Raman bands of the SWCNTs within the cement matrix. As a result, the concentrated mechanical compression on the SWCNTs induced shrinkage of the carbon-carbon bonds thereby resulting in the upshifted Raman bands [37,38]. The variation in the upshifted frequency of the G-band under the mechanical compression was very large which was possibly due to the ensemble nature (i.e., semiconducting and metallic) of the SWCNTs as well as the degree of the dispersion state of the tubes in the cement matrix. This result indicates that when SWCNTs are incorporated in the cement matrix individually, the strong Raman signals from the SWCNTs can be used as a strain sensor. In other words, it is possible to monitor non-destructively how cement composites behave under various mechanical loadings by using an optical apparatus from a remote distance.

4. Conclusions

We have demonstrated the adding effect of SWCNTs with a diameter below 1 nm for cement composites in terms of their optical sensitivity upon mechanical compression. To fully exploit the optical properties of the SWCNTs, we achieved a homogeneous dispersion of the SWCNTs in an aqueous solution with the aid of DNA wrapping. Through various optical tools and TEM micrographs, the highly dispersed state of the SWCNTs in distilled water was systematically analyzed. For the formation of hydrated crystals, there was no negative effect of the DNA on the hydration reaction when the added amount of DNA was below 0.075 wt%. Noticeably, the highest compressive strength of the cement composite was achieved when the added amount of DNA with respect to cement was ca. 0.05 wt%. It was expected that an appropriate amount of hydrophilic groups (e.g., -OH and $-NH_2$) act as anchoring sites for the growth of the hydrated crystals. In contrast, a dramatic retarding effect of the DNA on the hydration of the cement composites was observed when the added amount of DNA was extremely large over 0.1 wt%. DNA because a large number of hydrophilic groups has a high tendency to be adsorbed onto the surface of the cement particles thereby resulting in the retarded hydration reaction. Based on the XRD and in-situ Raman studies, the excess DNA that was added hindered the growth of calcium hydroxide and ettringite at the early state of the hydration reaction. Finally, we demonstrated the high sensitivity of the individually dispersed SWCNTs within the cement matrix upon mechanical compression. Our results suggest that this newly developed method is a novel approach to monitor non-destructively how cement composites behave under various mechanical loadings using an optical apparatus from a remote distance.

Conflict of Interest

No potential conflict of interest relevant to this article was reported.

Acknowledgements

Y.A.K. acknowledges the financial support from the National Research Foundation of Korea (NRF) grant funded by the Korea government (MSIP) (No. NRF-2017R1A2A1A17069771) and from the Nano · Material Technology Development Program through the NRF funded by the Ministry of Science, ICT and Future Planning (2016M3A7B4021149).

References

[1] Gagg RC. Cement and concrete as an engineering material: an historic appraisal and case study analysis. Eng Failure Anal, **40**, 114 (2014). https://doi.org/10.1016/j.engfailanal.2014.02.004.

[2] Li H, Xiao HG, Yuan J, Ou J. Microstructure of cement mortar with nano-particles. Compos Part B Eng, **35**, 185 (2004). https://doi.org/10.1016/S1359-8368(03)00052-0.

[3] Lilkov V, Rostovsky I, Petrov O, Tzvetanova Y, Savov P. Long term study of hardened cement pastes containing silica fume and fly ash. Constr Build Mater, **60**, 48 (2014). https://doi.org/10.1016/j.conbuildmat.2014.02.045.

[4] Horszczaruk E, Mijowska E, Cendrowski K, Mijowska S, Sikora P. Effect of incorporation route on dispersion of mesoporous silica nanospheres in cement mortar. Constr Build Mater, **66**, 418 (2014). https://doi.org/10.1016/j.conbuildmat.2014.05.061.

[5] Meng T, Yu Y, Qian X, Zhan S, Qian K. Effect of nano-TiO_2 on the mechanical properties of cement mortar. Constr Build Mater, **29**, 241 (2012). https://doi.org/10.1016/j.conbuildmat.2011.10.047.

[6] Li GY, Wang PM, Zhao X. Mechanical behavior and microstructure of cement composites incorporating surface-treated multi-walled carbon nanotubes. Carbon, **43**, 1239 (2005). https://doi.org/10.1016/j.carbon.2004.12.017.

[7] Saez de Ibarra Y, Gaitero JJ, Erkizia E, Campillo I. Atomic force microscopy and nanoindentation of cement pastes with nanotube dispersions. Phys Status Solidi A, **203**, 1076 (2006). https://doi.org/10.1002/pssa.200566166.

[8] Wansom S, Kidner NJ, Woo LY, Mason TO. AC-impedance response of multi-walled carbon nanotube/cement composites. Cem Concr Compos, **28**, 509 (2006). https://doi.org/10.1016/j.cemconcomp.2006.01.014.

[9] Li GY, Wang PM, Zhao X. Pressure-sensitive properties and microstructure of carbon nanotube reinforced cement composites. Cem Concr Compos, **29**, 377 (2007). https://doi.org/10.1016/j.cemconcomp.2006.12.011.

[10] Cwirzen A, Habermehl-Cwirzen K, Penttala V. Surface decoration of carbon nanotubes and mechanical properties of cement/carbon nanotube composites. Adv Cem Res, **20**, 65 (2008). https://doi.org/10.1680/adcr.2008.20.2.65.

[11] Han B, Yu X, Kwon E. A self-sensing carbon nanotube/cement composite for traffic monitoring. Nanotechnology, **20**, 445501 (2009). https://doi.org/10.1088/0957-4484/20/44/445501.

[12] Musso S, Tulliani JM, Ferro G, Tagliaferro A. Influence of carbon nanotubes structure on the mechanical behavior of cement composites. Compos Sci Technol, **69**, 1985 (2009). https://doi.org/10.1016/j.compscitech.2009.05.002.

[13] Konsta-Gdoutos MS, Metaxa ZS, Shah SP. Highly dispersed carbon nanotube reinforced cement based materials. Cem Concr Res, **40**, 1052 (2010). https://doi.org/10.1016/j.cemconres.2010.02.015.

[14] Siddique R, Mehta A. Effect of carbon nanotubes on properties of cement mortars. Constr Build Mater, **50**, 116 (2014). https://doi.org/10.1016/j.conbuildmat.2013.09.019.

[15] Lv S, Ma Y, Qiu C, Sun T, Liu J, Zhou Q. Effect of graphene oxide nanosheets of microstructure and mechanical properties of cement composites. Constr Build Mater, **49**, 121 (2013). https://doi.org/10.1016/j.conbuildmat.2013.08.022.

[16] Rhee I, Kim YA, Shin GO, Kim JH, Muramatsu H. Compressive strength sensitivity of cement mortar using rice husk-derived graphene with a high specific surface area. Constr Build Mater, **96**, 189 (2015). https://doi.org/10.1016/j.conbuildmat.2015.08.016.

[17] Makar JM, Chan GW. Growth of cement hydration products on single-walled carbon nanotubes. J Am Ceram Soc, **92**, 1303 (2009). https://doi.org/10.1111/j.1551-2916.2009.03055.x.

[18] Li X, Wei W, Qin H, Hu YH. Co-effects of graphene oxide sheets and single wall carbon nanotubes on mechanical properties of cement. J Phys Chem Solids, **85**, 39 (2015). https://doi.org/10.1016/j.jpcs.2015.04.018.

[19] Dresselhaus MS, Dresselhaus G, Eklund PC. Science of Fullerenes and Carbon Nanotubes, Academic Press, San Diego (1996).

[20] Kim YA, Yang KS, Muramatsu H, Hayashi T, Endo M, Terrones M, Dresselhaus MS. Double-walled carbon nanotubes: synthesis, structural characterization, and application. Carbon Lett, **15**, 77 (2014). http://dx.doi.org/10.5714/CL.2014.15.2.077.

[21] Lin Y, Taylor S, Li H, Shiral Fernando KA, Qu L, Wang W, Gu L, Zhou B, Sun YP. Advances toward bioapplications of carbon nanotubes. J Mater Chem, **14**, 527 (2004). https://doi.org/10.1039/B314481J.

[22] Lee Y, Geckeler KE. Carbon nanotubes in the biological interphase: the relevance of noncovalence. Adv Mater, **22**, 4076 (2010). https://doi.org/10.1002/adma.201000746.

[23] Karajanagi SS, Yang H, Asuri P, Sellitto E, Dordick JS, Kane RS. Protein-assisted solubilization of single-walled carbon nanotubes. Langmuir, **22**, 1392 (2006). https://doi.org/10.1021/la0528201.

[24] Nepal D, Geckeler KE. pH-sensitive dispersion and debundling of single-walled carbon nanotubes: lysozyme as a tool. Small, **2**, 406 (2006). https://doi.org/10.1002/smll.200500351.

[25] Kim JH, Kataoka M, Kim YA, Shimamoto D, Muramatsu H, Hayashi T, Endo M, Terrones M, Dresselhaus MS. Diameter-selective separation of double-walled carbon nanotubes. Appl Phys Lett, **93**, 223107 (2008). https://doi.org/10.1063/1.3039790.

[26] Kim JH, Kataoka M, Shimamoto D, Muramatsu H, Jung YC, Tojo T, Hayashi T, Kim YA, Endo M, Terrones M, Dresselhaus MS. Defect-enhanced dispersion of carbon nanotubes in DNA solutions. Chem Phys Chem, **10**, 2414 (2009). https://doi.org/10.1002/cphc.200900362.

[27] Kim JH, Kataoka M, Shimamoto D, Muramatsu H, Jung YC, Hayashi T, Kim YA, Endo M, Park JS, Saito R, Terrones M, Dresselhaus MS. Raman and fluorescence spectroscopic studies of a DNA-dispersed double-walled carbon nanotube solution. ACS Nano, **4**, 1060 (2010). https://doi.org/10.1021/nn901871g.

[28] O'Connell MJ, Boul P, Ericson LM, Huffman C, Wang Y, Haroz E, Kuper C, Tour J, Ausman KD, Smalley RE. Reversible water-solubilization of single-walled carbon nanotubes by polymer wrapping. Chem Phys Lett, **342**, 265 (2001). https://doi.org/10.1016/S0009-2614(01)00490-0.

[29] O'Connell MJ, Bachilo SM, Huffman CB, Moore VC, Strano MS, Haroz EH, Rialon KL, Boul PJ, Noon WH, Kittrell C, Ma J, Hauge RH, Weisman RB, Smalley RE. Band gap fluorescence from individual single-walled carbon nanotubes. Science, **297**, 593 (2002). https://doi.org/10.1126/science.1072631.

[30] Heller DA, Barone PW, Swanson JP, Mayrhofer RM, Strano MS. Using Raman spectroscopy to elucidate the aggregation state of single-walled carbon nanotubes. J Phys Chem B, **108**, 6905 (2004). https://doi.org/10.1021/jp037690o.

[31] Strano MS, Moore VC, Miller MK, Allen MJ, Haroz EH, Kittrell C, Hauge RH, Smalley RE. The role of surfactant adsorption during ultrasonication in the dispersion of single-walled carbon nanotubes. J Nanosci Nanotechnol, **3**, 81 (2003). https://doi.org/10.1166/jnn.2003.194.

[32] Bullard JW, Jennings HM, Livingston RA, Nonat A, Scheer GW, Schweitzer JS, Scrivener KL, Thomas JJ. Mechanisms of cement hydration. Cem Concr Res, **41**, 1208 (2011). https://doi.org/10.1016/j.cemconres.2010.09.011.

[33] Liu F, Sun Z, Qi C. Raman spectroscopy study on the hydration behaviors of Portland cement pastes during setting. J Mater Civ Eng, **27**, 04014223 (2014).

[34] Deng CS, Breen C, Yarwood J, Habesch S, Phipps J, Craster R, Maitland G. Ageing of oilfield cement at high humidity: a combined FEG-ESEM and Raman microscopic investigation. J Mater Chem, **12**, 3105 (2002). https://doi.org/10.1039/B203127M.

[35] Shoda M, Bandow S, Maruyama Y, Iijima S. Probing interaction between ssDNA and carbon nanotubes by Raman scattering and electron microscopy. J Phys Chem C, **113**, 6033 (2009). https://doi.org/10.1021/jp8109572.

[36] Cha M, Jung S, Cha MH, Kim G, Ihm J, Lee J. Reversible metal−semiconductor transition of ssDNA-decorated single-walled carbon nanotubes. Nano Lett, **9**, 1345 (2009). https://doi.org/10.1021/nl8029948.

[37] Andrade NF, Aguiar AL, Kim YA, Endo M, Freire PTC, Brunetto G, Galvão DS, Dresselhaus MS, Souza Filho AG. Linear carbon chains under high-pressure conditions. J Phys Chem C, **119**, 10669 (2015). https://doi.org/10.1021/acs.jpcc.5b00902.

[38] Venkateswaran UD, Rao AM, Richter E, Menon M, Rinzler A, Smalley RE, Eklund PC. Probing the single-wall carbon nanotube bundle: Raman scattering under high pressure. Phys Rev B, **59**, 10928 (1999).